An Anthropomorphic Robotic Finger With Innate Human-Finger-Like Biomechanical Advantages Part II: Flexible Tendon Sheath and Grasping Demonstration

Yiming Zhu, Guowu Wei, *Member, IEEE*, Lei Ren, *Member, IEEE*, Zirong Luo, and Jianzhong Shang

***Abstract*—The human hand has a fantastic ability to interact with various objects in the dynamic unstructured environment of our daily activities. We believe that this outstanding performance benefits a lot from the unique biological features of the hand musculoskeletal system. In Part I of this article, a bio-inspired anthropomorphic robotic finger was developed, based on which two human-finger-like biomechanical advantages were elaborately investigated, including the anisotropic variable stiffness associated with the ligamentous joints and the enlarged feasible force space associated with the reticular extensor mechanisms. In Part II, the fingertip force-velocity characteristics resulting from the flexible tendon sheath are studied. It indicates that the fingertip force–velocity workspace can be greatly augmented owing to the self-adaptive morphing of the flexible tendon sheaths, showing the average improvement of 41.2% theoretically and 117.5% experimentally compared with the results of 2 mm, 4 mm, and 6 mm size rigid tendon sheaths. Grasping tests and comparisons are then conducted with four three-fingered robotic hands (one with the robotic finger proposed in Part I, one with hinge joints, one with linear extensors, and one with rigid tendon sheaths) and the human hands of six subjects to handle various objects on flat, rough, and soft surfaces. The results show that the novel bio-inspired design in this research could improve the grasping success rates of the robotic hand. Compared with the grasping test results from the robotic hand with the bio-inspired robotic finger proposed in Part I, the overall grasping performance of a robotic hand with hinge joints, linear extensors, and rigid tendon sheaths decreases by 10%, 6%, and 17%, respectively. The results have also shown that with the embedded biomechanical advantages, even without complex control and sensory systems, the robotic fingers can achieve very comparable performance to human fingers in the grasping demonstrations presented, indicating average 94% of the success rate achieved by the human fingers. Successfully demonstrating 14 of 16 grasp types in the Cutkoskey taxonomy further shows the human-finger-like grasping capability of the proposed robotic fingers.**

***Index Terms*—Bio-inspired robotic finger, flexible tendon sheath, force–velocity workspace, robotic hand, grasping and manipulation.**

Manuscript received 19 May 2022; accepted 16 July 2022. Date of publication 9 September 2022; date of current version 8 February 2023. This work was supported in part by the project of National Key R&D Program of China under Grant 2018YFC2001300 and in part by the project of National Natural Science Foundation of China under Grant 91948302, Grant 91848204, Grant 52005209, and Grant 51675222. This article recommended for publication by Associate Editor F. Ficuciello and Editor E. Yoshida upon evaluation of the reviewers' comments. (*Corresponding authors: Guowu Wei; Lei Ren.*)

Yiming Zhu is with the School of Mechanical, Aerospace and Civil Engineering, The University of Manchester, Manchester M13 9PL, U.K., and also with the College of Intelligence Science and Technology, National University of Defense Technology, Changsha 410073, China (e-mail: yiming.zhu@manchester.ac.uk).

Guowu Wei is with the School of Science, Engineering and Environment, University of Salford, M5 4WT Salford, U.K. (e-mail: g.wei@salford.ac.uk).

Lei Ren is with the School of Mechanical, Aerospace and Civil Engineering, The University of Manchester, M13 9PL Manchester, U.K., and also with the Key Laboratory of Bionic Engineering, Ministry of Education, Jilin University, Changchun 130012, China (e-mail: lei.ren@manchester.ac.uk).

Zirong Luo and Jianzhong Shang are with the College of Intelligence Science and Technology, National University of Defense Technology, Changsha 410073, China (e-mail: luozirong@nudt.edu.cn; jz_shang_nudt@163.com).

This article has supplementary material provided by the authors and color versions of one or more figures available at https://doi.org/10.1109/TRO.2022.3200143.

Digital Object Identifier 10.1109/TRO.2022.3200143

I. Introduction

THE human hand is a powerful and multifunctional tool. During the interaction with objects, except for the dominant control command from the brain, our hands can autonomously adapt their posture, stiffness, contact force, and velocity according to different object shapes, dimensions, weights, softness, as well as different environments. For example, when grasping a baseball, our fingers will autonomously adjust the palmar orientation to make a larger contact area so that a more stable grasp can be obtained. In our daily lives, our hands are capable of picking up a peanut, a pen, or grasping an apple, a bottle, even without consciously differentiating the motion control command. These interactions often happen in dynamic, irregular, unstructured, and uncertain environments, such as on smooth or rough, soft or rigid surfaces. Moreover, our hands can also perform numerous complex manipulations, such as playing an instrument or performing surgical procedures, thanks to their intrinsic advanced dexterity and versatility.

We believe that the musculoskeletal structures of the hand provide basic and crucial conditions for its excellent performance, inspiring the novel design of robotic hands. Modern robotic hands have been studied for about five decades [1]. Though many advancements have been made, the grasping and especially manipulation abilities of the current robotic hands still cannot match human hands. This might be due to the lack of fully understanding the biomechanical advantages of the human hand and exploiting them in the development of robotic hands. We hypothesize that there must be some underlying

relationships between the versatile performance of the human hand and its biomechanical mechanisms. To figure out the underlying biomechanical principles and adopt these biological mechanisms on the robotic hand/finger design, in Part I of this article, an anthropomorphic robotic finger was developed, and using it the biomechanical advantages of the ligamentous joint and the extensor mechanism were revealed through theoretical analysis and experimental verification. Results from Part I have shown that the anisotropic variable joint stiffness could be obtained through ligamentous joint design and the fingertip feasible force space could be enlarged by the reticular extensor mechanism. Moreover, for accomplishing proficient grasping and manipulation tasks, the fingertip force–velocity relationship is continuously altered. This force–velocity relationship is described as force–velocity workspace and is adjusted through the transmission system, i.e., the flexible tendon sheaths. In this part, by using the bio-inspired robotic finger developed in Part I of this article, the fingertip force–velocity characteristics related to the flexible tendon sheath are systematically investigated through mathematical modeling and experimental verification. It is found that

1) Benefitting from its self-adaptive morphing function, the flexible tendon sheath can autonomously adjust the moment arm of the joint, resulting in the enlargement of the fingertip force–velocity workspace.

Further, to better illustrate how the human-finger-like structures influence the robotic fingers' performance, grasping tests are then conducted on a three-fingered robotic hand that is built based on the proposed robotic finger. To make the comparison, three additional robotic hands with some specific different structures were designed and developed. One of these additional robotic hand has hinge joints in the finger, to replace the ligamentous joints [see Fig. 3(c)]. The second additional robotic hand has linear extensors in the finger [see Fig. 3(d)], replacing the reticular extensors in the original design. The third additional robotic hand uses the rigid tendon sheaths in the finger [see Fig. 3(e)], instead of the flexible tendon sheaths. Every prototype was then mounted on the same actuation platform to complete the grasping tasks. The results show that the ligamentous joint, the reticular extensor and the flexible tendon sheath could all help improve the grasping capability of robotic fingers, especially the flexible tendon sheath structure. Specifically, compared with the robotic hand with the proposed highly biomimetic design, the grasping success rates of the robotic hands with hinge joints, linear extensors, and rigid tendon sheaths, respectively, decreased 10%, 6%, and 17% on average in the proposed grasping tests. The comparison results with the human fingers indicates that, even without complex control or learning algorithms, the proposed bio-inspired robotic fingers can perform human-finger-like grasping performance in the tests presented, showing average 94% of the success rate achieved by the human fingers.

This article for the first time studies the influence of the properties of the tendon sheath structure on the quasi-static and dynamic behaviors of the finger. The mathematical model of the flexible tendon sheaths system is for the first time proposed for the theoretical analysis. The quick-release test is innovatively adopted to investigate the dynamic characteristics of the fingertip. In addition, the individual impact of the ligamentous joint, the reticular extensor, and the flexible tendon sheath on the grasping performance is for the first time demonstrated with the specific percentage of improvement obtained. This article will not only lay the groundwork for further research into biomechanics of human fingers/hands, but also inspire the better design of robotic fingers/hands.

II. Related Work

The force–velocity characteristics are often used to describe the mechanical output power of actuators (muscles or motors) and end-effectors in biomechanics [2], [3] and robotics research [4], [5]. It has important implications for evaluating human muscle efficiency and fatigue [3]. The hyperbolic-like force–velocity relationships of human muscles were normally found by researchers in biomechanics and kinesiology [6], [7]. Haeufle et al. [8] and Schmitt et al. [9] adopted a quick-release test to measure the biological muscle characteristics and had obtained similar hyperbolic force–velocity relationships. In the robotic systems, O'Brien et al. [5] designed an elastomeric passive transmission pulley to optimize the robotic finger's force and velocity outputs. The pulley could autonomously adjust its radius according to the tension on the actuation string. In their work, the fingertip force and velocity were tested separately, and no dynamic force–velocity characteristics were investigated as those in the human muscles research. Their work provided an idea that the endpoint force–velocity characteristics could be adjusted through the design of the transmission system between the actuators and the end effectors. Such a transmission system exists in human hands which is functioned by the pulley-like flexible tendon sheath structure. We believe that the flexible tendon sheath structure potentially plays a role in regulating and optimizing the fingertip force–velocity characteristics. Amis and Jones [10] revealed the detailed structure of tendon sheaths and found their bulging behavior during flexion. Lin [11] investigated the mechanical properties of the pulley-like tendon sheath system and explained its constraint function of the tendons in preventing bow-stringing behavior. Some researchers have tried to mimic the tendon sheath structure in robotic hand design. Xu and Todorov [12] built simplified tendon sheaths by using laser-cut rubber sheets in the development of an anthropomorphic robotic hand and briefly introduced the function of the elastic tendon sheath in adjusting the moment arm of the finger joint. In other biomimetic robotic hand designs, Chepisheva et al. [13] used PTFE tubes as tendon pulleys, and Mohd Faudzi et al. [14] used polyethylene tubes as tendon sheaths, which were both made from rigid materials. Tebyani et al. [15] printed the tendon sheaths together with the bones by using some flexible printing materials. Though researchers have attempted to adopt the tendon sheath structure of human fingers in the design of robotic hands, no detailed study has been conducted to investigate how the flexible tendon sheath influences the fingertip force–velocity characteristics, no matter on human hands or robotic hands. In this part of this article, we will investigate the impact of the flexible tendon sheath on the fingertip force–velocity characteristics

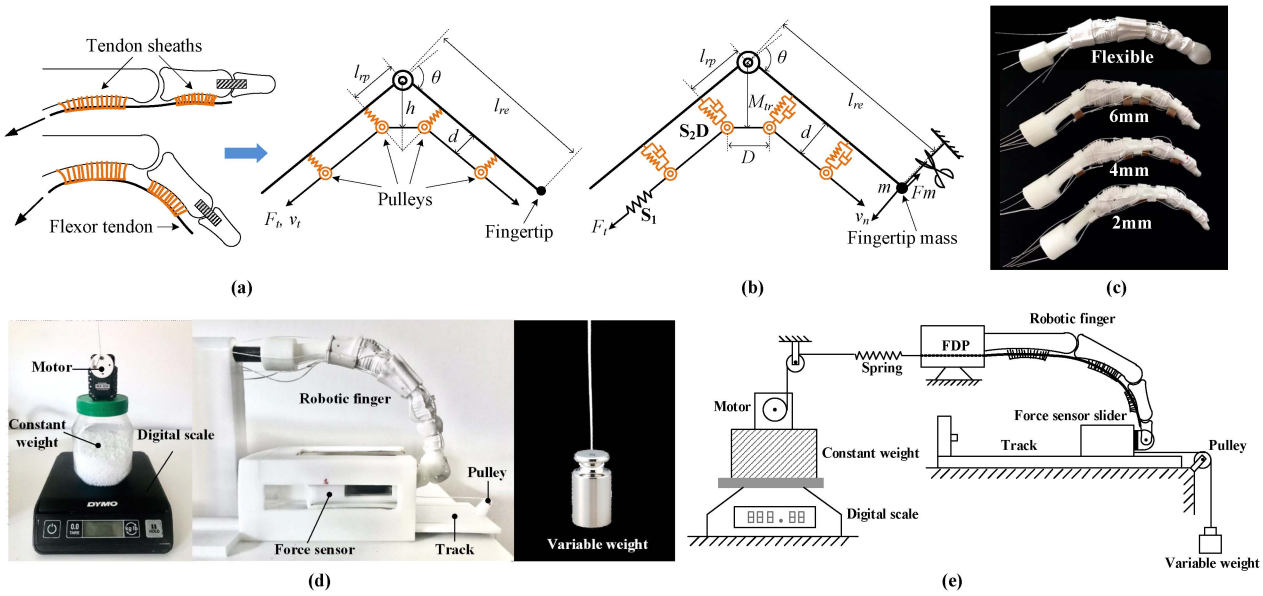

Fig. 1. Modeling and experiment about the impact of flexible tendon-sheath on fingertip force–velocity characteristics. (a) The schematic diagram of the single-joint elastic tendon sheath pulley system (for quasi-static analysis); (b) the schematic diagram of the quick-release experiment on the single-joint model (for dynamic analysis); (c) the robotic finger model with the flexible tendon sheath and three comparison robotic finger models with rigid tendon sheaths of different thicknesses (6 mm, 4 mm, and 2 mm); (d) the test rig for the quick-release experiment; (e) the schematic diagram of the quick-release test rig.

in detail through both theoretical modeling and experimental study.

III. Augmented Force-Velocity Workspace Associated With the Flexible Tendon Sheath

The flexible tendon sheaths can flatten down to hold the tendons affixing to the phalanges when the finger straightens, resulting in small initial moment arms at the joints. This allows a fast-bending motion with slight flexion torques. Meanwhile, the tendon sheaths can bulge out to accommodate the tendons and locate them a distance away from the phalanges when the finger bends. This leads to the increase of the moment arms at the joints to generate large flexion torques with low bending speed [10]. Concerning these behaviors, the flexible tendon sheath system is expected to show a similar force–velocity self-adaption function to the elastomeric passive transmission systems discovered in the research of O'Brien et al. [5]. Hence, in this section, both mathematical models and experimental studies are carried out to investigate the impact of the flexible tendon sheath as well as the rigid tendon sheaths of various sizes on the force–velocity characteristics of a finger.

A. Mathematical Model

Both quasi-static and dynamic performance contributed by the tendon sheath are investigated in this section. Here, the quasi-static force-and-velocity characteristics describe the maximal endpoint force and velocity that the finger can achieve. For one pair of quasi-static force–velocity values, they respectively correspond to the extremum force and the extremum velocity on the entire curve. Thus, this pair of values is normally obtained from the two endpoints of the curve. The reason we call them the quasi-static force and velocity characteristics is that the endpoint velocity can be extremely low (nearly static) when generating the maximal force, and the endpoint force can be approximate to zero (nearly no resistance) when outputting the maximal velocity. While the dynamic force–velocity characteristics are the practical working points on the curve, representing the endpoint force and velocity that the mechanism can simultaneously produce during work. In fact, the working curve itself is a graphical description of the mechanism's dynamic force–velocity characteristics. Both of the quasi-static and dynamic characteristics can show the system properties from different aspects [5], [16], [17]. Therefore, both quasi-static and dynamic mathematical models for characterizing the impact of the flexible tendon sheath on the fingertip force–velocity characteristics are presented as follows.

For the quasi-static analysis, let us consider one finger joint (PIP joint) as shown in Fig. 1(a). In this model, a tendon held by the tendon sheaths is equivalently treated as a tendon held by two elastic pulleys on each of the two adjacent phalanges. Here, we make an assumption that the DIP joint is fixed at the zero-angle position. In Fig. 1(a), θ is the PIP joint flexion angle, l_{rp} is the distance from the pulley edge to the rotation axis, d is the distance between the tendon and the phalanx, h is the distance from the tendon to the rotation axis, which equals to the moment arm M_{tr}, l_{re} is the distance from the PIP joint center to the fingertip, F_t is the tendon force, and v_t is the tendon excursion velocity.

Referring to Fig. 1(a), the moment arm from the tendon to the rotation axis can be derived as

$$M_{tr} = h = \frac{l_{rp}}{\sin(\theta/2)} - \left(\frac{l_{rp}}{\tan(\theta/2)} - d\right)\cos\left(\frac{\theta}{2}\right). \quad (1)$$

In the quasi-static analysis, the viscous damping effects of the tendon sheath can be ignored since there will be no force generated by the viscous damping element in the condition of quasi-static velocity. Thus, given that the elastic coefficient of the pulley spring is k_p, and the initial length of the spring is d_0, the relationship between the tendon force F_t, and the distance d can be expressed as

$$d = d_0 + \frac{F_t \sin(\theta/2)}{k_p} \tag{2}$$

where d must satisfy that $d \leq \dfrac{l_{rp}}{\tan(\theta/2)}$.

Then, the moment arm M_{tr} can be further formulated as

$$M_{tr} = l_{rp} \sin\left(\frac{\theta}{2}\right) + d_0 \cos\left(\frac{\theta}{2}\right) + \frac{F_t}{k_p} \sin\left(\frac{\theta}{2}\right) \cos\left(\frac{\theta}{2}\right) \tag{3}$$

where l_{rp}, d_0, and k_p are all constants during the flexion motion, which are only related to the anatomical structure of the finger.

It can be seen from (3) that the moment arm increases as the tendon force and the joint's flexion angle increase. In this equation, the first two terms can be considered as the kinematic effects on the moment arm. And the last term can be regarded as the effect of the elastic and flexible properties of the tendon sheaths on the moment arm. Obviously, in the case when a rigid tendon sheath is considered, the tendon force will not change the moment arm, as in this case, k_p becomes infinity and thus the last term in (3) is neglectable. In (3), there is an assumption that the moment arm M_{tr} is no less than the initial length of the spring d_0, with the minimum value d_0 occurring when the finger straightens ($\theta = 0$).

Then, the joint angular velocity ω_r and torque τ_r can be calculated as

$$\omega_r = \frac{v_t}{M_{tr}}, \tau_r = F_t M_{tr}. \tag{4}$$

Using (4), the fingertip normal velocity v_n and force F_n can be deduced as

$$\begin{cases} v_n = \omega_r l_{re} = \frac{v_t}{M_{tr}} l_{re} \\ F_n = \frac{\tau_r}{l_{re}} = \frac{F_t M_{tr}}{l_{re}}. \end{cases} \tag{5}$$

The above equation provides the quasi-static model that relates the fingertip velocity and force. By substituting the structure parameters into the above equations, the quasi-static velocity–force relation affected by the property of the tendon sheath can be characterised and illustrated.

For the robotic finger with the flexible tendon sheath designed in Part I of this article, the structure and physical parameters are as $l_{rp} = 6$ mm, $l_{re} = 25$ mm, $d_0 = 2$ mm, $k_p = 0.6$ N/mm, $F_t = 6$ N, and $v_t = 50$ mm/s. Substituting these parameters into (3) and (5), the relationships between the fingertip velocity and flexion angle as well as the fingertip force and flexion angle can be obtained.

In addition, for the purpose of comparison, rigid tendon sheaths with the size of $d_0 = 2$ mm, 4 mm, and 6 mm are considered. With the other parameters being the same as that of the flexible tendon sheath, the corresponding relationships for the fingertip velocity and force can also be characterised through (3) and (5), but in this case, the last term in (3) is zero as k_p is much greater than F_t.

The simulation results are illustrated in Fig. 2(a) and (b). As can be seen in the figure, with the flexible tendon sheath, the finger can achieve high fingertip velocity when the flexion angles are small [see Fig. 2(a)], and meanwhile, it can generate large fingertip forces around the full flexion regions [see Fig. 2(b)]. However, for the finger with the rigid tendon sheaths, only one of the situations can be achieved, e.g., the larger size of the tendon sheath, the larger fingertip force but the lower fingertip velocity. Further, for each rigid tendon sheath with the sizes from 2 mm to 6 mm, the maximal values of the fingertip force and velocity are calculated and represented as the solid curve shown in Fig. 2(c), with the velocity being the x-value and the force giving the y-value. Likewise, the maximal values of the fingertip force and velocity of the robotic finger with the flexible tendon sheath are also calculated and marked as one point denoted with a red "+" (which is overlapped with the red circle point). It should be noted that to make a rational comparison, all the values in the x-coordinates are normalized with respect to the maximum fingertip velocity of the flexible tendon sheath, and all the values in the y-coordinates are normalized with respect to the maximum fingertip force of the flexible tendon sheath.

As can be seen in Fig. 2(c), a rigid thin tendon sheath allows high fingertip velocity but poor force-generating capability. Conversely, if the size of the tendon sheath is great, it can produce a large fingertip force but low velocity since the tendon cannot be held close to the phalanx even at the initial phase of the finger flexion. When a flexible tendon sheath is used, the force–velocity property of the finger is greatly improved. As shown by the red cross mark in Fig. 2(c), it illustrates that the finger is capable of achieving both high fingertip velocity and large fingertip force due to the additional moment arm regulation function of the flexible tendon sheath.

Next, the dynamic force–velocity characteristics affected by different tendon sheaths are investigated. To obtain the dynamic characteristics of the fingertip force–velocity output, a quick-release test is constructed and simulated in the theoretical model in this section. The approach employed herein is commonly used to investigate the force–velocity relation of muscle contraction or bio-inspired actuators [2], [8], [9]. The schematic diagram of the quick-release experiment on the single-joint (PIP joint) model is shown in Fig. 1(b). The DIP joint angle here is also assumed to be zero and constant. During the whole release process of this model, l_{rp} is the distance from the pulley edge to the rotation axis, l_{re} is the distance from the PIP joint center to the fingertip, θ represents the PIP joint flexion angle, d represents the distance between the tendon and the phalanx, M_{tr} is the distance from the tendon to the rotation axis, which is also the corresponding moment arm, F_t is the tendon force, D is the distance between the tendon sheath ends on the two sides of the joint, m is the mass attached on the fingertip, v_n is the velocity

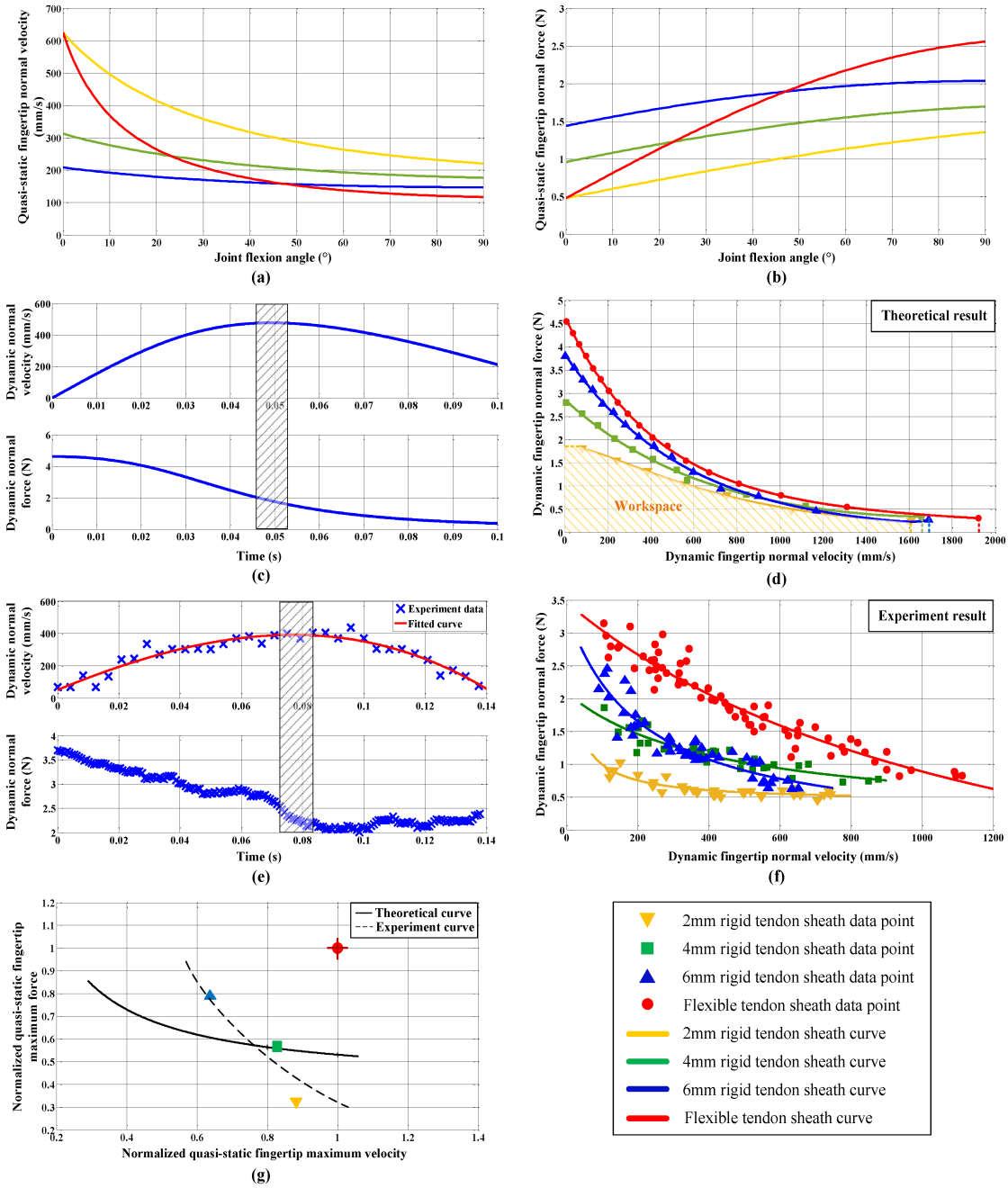

Fig. 2. Theoretical and experiment results of the fingertip force-velocity characteristics with different tendon sheaths. (a) The quasi-static relationship between the fingertip normal velocity and the joint flexion angle; (b) the quasi-static relationship between the fingertip normal force and the joint flexion angle; (c) fingertip force and velocity theoretical results with the flexible tendon sheath in a 180 g load; (d) the comparison results of the dynamic force–velocity characteristics with different tendon sheaths in single-joint theoretical models; (e) fingertip force and velocity experiment results with the flexible tendon sheath in a 180 g load; (f) dynamic force–velocity characteristics of the four physical robotic finger models; (g) the normalized results of the theoretical and experiment data about the quasi-static maximum force and velocity that different finger models can output. (Note: Yellow for 2 mm rigid tendon sheath; green for 4 mm rigid tendon sheath; blue for 6 mm rigid tendon sheath; and red for flexible tendon sheath).

of the fingertip, and F_m is a constant external resistance force applied to the fingertip in the normal direction, which equals to mg. As the system is constructed on a horizontal plane, the influence from gravity can be neglected in this model. S_1 is a spring element, and S_2D is a spring damping element. It should be noted that the tendon sheath model here is different from the one in the quasi-static analysis. In the dynamic condition, the velocity of the tendon sheath will induce viscous damping effects. And the force contributed by this damping element cannot be ignored during the dynamic analysis. Therefore, the tendon sheath model in Fig. 1(b) consists of an elastic element and a parallel damping element.

To obtain the dynamic fingertip normal force and velocity output when the system reaches the steady state after releasing, we referred to the method used in [8]. This method can demonstrate the variation of the fingertip force and velocity during the whole

release process. And it can be formulated as

$$\begin{cases} F_t \sin\left(\frac{\theta}{2}\right) = k_2 \left(d - d_0\right) + cd' \\ M_{tr} = l_{rp} \sin\left(\frac{\theta}{2}\right) + d\cos\left(\frac{\theta}{2}\right) \\ \frac{F_t M_{tr}}{l_{re}} = m l_{re} \theta'' + F_m \\ F_{ti} - F_t = k_1 \left(D_i - D\right) \\ F_n = \frac{F_t M_{tr}}{l_{re}} \\ v_n = l_{re} \theta' \end{cases} \tag{6}$$

where

$$\begin{cases} D = 2\left(l_{rp}\cos\left(\frac{\theta}{2}\right) - d\sin\left(\frac{\theta}{2}\right)\right) \\ D_i = 2\left(l_{rp}\cos\left(\frac{\theta_i}{2}\right) - d_i\sin\left(\frac{\theta_i}{2}\right)\right) \\ F_{ti}\sin\left(\frac{\theta_i}{2}\right) = k_2\left(d_i - d_0\right). \end{cases} \tag{7}$$

Equations (6) and (7) are both obtained from the fundamental force and geometrical conditions of the model. Throughout the release process, only l_{rp}, l_{re}, m, and F_m are constant, and all the other parameters will continually change after release. In (6) and (7), k_1 and k_2 are the elastic coefficients of the elements S_1 and $\mathrm{S}_2\mathrm{D}$, c is the viscous damping coefficient of the element $\mathrm{S}_2\mathrm{D}$, d_0 is the tendon sheath original size, d' is the tendon sheath contraction velocity, θ' and θ'' are, respectively, the PIP joint angular velocity and angular acceleration, F_n and v_n are, respectively, the fingertip normal force and velocity, F_{ti} is the initial tendon force before release, D_i is the initial distance between the tendon sheath ends on the two sides of the joint before release, d_i is the initial distance between the tendon, and the phalanx before release, and θ_i is the initial joint angle before release.

With the above derivation, numerical simulations are conducted to illustrate the dynamic impact of the flexible tendon sheath on the finger force–velocity behavior. These two sets of differential equations were solved by using the ode45 tool box embedded in MATLAB. The parameters used in the derivation can be obtained from the geometries and material properties of the robotic finger structures. They were $l_{rp} = 6$ mm, $l_{re} = 25$ mm, $d_0 = 2$ mm, $\theta_i = 30°$, $k_1 = 1.7$ N/mm, $k_2 = 0.6$ N/mm, $c = 2 \times 10^{-4}$ Ns/mm, and $F_{ti} = 13$ N. The dynamic force–velocity output analysis was conducted in various fingertip load conditions, with the fingertip mass m varying in the range from 30 to 455 g with an increasing step of 25 g. The external resistance force F_m thus accordingly changes from 0.3 to 4.55 N with the gravitational acceleration $g = 10$ m/s^2. This fingertip load range was selected since a larger load will exceed the loading capability of the finger in the initial tendon force condition. This will make the fingertip move in the opposite direction after release. A smaller load will make the fingertip keep accelerating during the whole release process in the finger joint motion range.

With (6) and (7), the fingertip normal force and velocity during the whole release process can be calculated. Taking the test with a 180 g fingertip load as an example, the fingertip normal velocity and force variation process is demonstrated in Fig. 2(c). It can be seen that the velocity gradually increases to a short peak plateau and then slowly declines. Correspondingly, the fingertip force keeps decreasing from the initial maximum value. It is suggested that the steady-state velocity and force outputs appear when the velocity is in the peak plateau stage [8]. This time period is marked as the shadowed block in Fig. 2(c). Thus, the steady-state velocity v_{180} was calculated as the average value of the velocities in this period. Likewise, the steady-state force F_{180} can be calculated as the average value of the forces in this period. In this way, we got a pair of data (v_{180}, F_{180}) to describe the dynamic velocity and force work point of the robotic finger in the 180 g load condition. Therefore, we can obtain a series of points by changing the fingertip load, and they were fitted by an exponential function, which is presented by the red curve in Fig. 2(d).

For the finger with rigid tendon sheaths, the elastic coefficient k_2 in (6) and (7) is assumed to be infinity. Thus, the distance between the tendon and the phalanx d is constant and always equals to the size of the tendon sheath d_0. By setting the tendon sheath size d_0 as 2 mm, 4 mm, and 6 mm, and using the other parameters the same as those for the flexible tendon sheath analysis, theoretical dynamic force–velocity characteristics of the finger with these three rigid tendon sheaths can be calculated and illustrated as shown in Fig. 2(d) (as yellow, green, and blue curves, respectively). Referring to Fig. 2(d), the force–velocity workspace is defined as the area enveloped by the characteristic curve and the two coordinate axes, in which all the force–velocity working points can be achieved by the robotic finger. Taking the curve of the 2 mm rigid tendon sheath as an example, in the range with the velocity of 82–1600 mm/s (calculated by the allowed fingertip load), the workspace is indicated as the yellow shadowed area. This workspace is much smaller than the area under the red curve, which is associated with the flexible tendon sheath. It can be obviously seen in the figure that the dynamic force–velocity characteristic curve with the flexible tendon sheath lays above the other curves with rigid tendon sheaths, implying the flexible property of the tendon sheath can theoretically enlarge the force–velocity workspace of a finger. These results are verified with experiments in the following section.

B. Experimental Verification

In this section, experiments are carried out to verify the theoretical analysis and simulation presented in the previous section. Since the quasi-static force–velocity output can be obtained from the two ends of the dynamic working curve, only dynamic force–velocity characteristics are tested in this section. In order to illustrate the influence of the flexibility of tendon sheath on the force–velocity workspace of a finger, for the purpose of comparison, three additional robotic fingers with rigid tendon sheaths of sizes 2 mm, 4 mm, and 6 mm were designed and fabricated, as shown in Fig. 1(c). To verify the prediction of the theoretical model, the quick-release experiments were conducted. The test rig is shown in Fig. 1(d) and (e). From left to right in Fig. 1(e), the test rig contains a digital scale, a constant weight, a motor, a connection spring, a robotic finger with the FDP tendon, a force sensor slider, a track, a pulley, and a variable weight. For the purpose of controlling the variables, the initial tendon force was set the same for different finger model tests, which was achieved by binding a constant weight with a motor that was

connected with a spring. The weight was placed on a digital scale to precisely read the value of the initial tendon force. The spring was linked with the FDP tendon of the robotic finger, and the fingertip was fixed to the press button of the force sensor through a revolute joint. The force sensor slider, which is a piece of calibrated force-sensing resistor (FSR) integrated with an Arduino Nano Every board, can only slide along the track horizontally so as to keep the testing press force and velocity in a constant direction. At the other end, a variable weight was connected with the force sensor slider through a pulley to provide a variable fingertip load.

At the beginning of the test, the posture of the robotic finger was set as 10° for the DIP joint, 30° for the PIP joint, 30° for the MCP flexion joint, and 0° for the MCP abduction joint. The variable weight was fixed so that the position of the fingertip did not change as long as the initial tendon force was set. The motor attached on the constant weight pulled the spring to exert the tendon force to a predefined value. The initial tendon force was set as 13 N, such that the fingertip could reach a steady state during the motion with both small and large fingertip loads. The digital scale showed the instantaneous force value, which equals the gravity of the constant weight subtracting the tendon force. For instance, if the constant weight used is 2 kg, the motor should rotate to pull the spring until the digital scale shows 700 g (the corresponding force 7 N converted from the readings on the digital scale 700 g equals to the gravity of the constant weight of 20 N subtracting the tendon force of 13 N).

After that, the variable weight was released, and the dynamic fingertip force and velocity were recorded. During the test, the Arduino board integrated into the FSR was set to collect the force data at a 500000-baud rate in real-time. The velocity of the slider was recorded by a high-speed camera at 960 frames per second (fps) and then analyzed in ImageJ with a Manual Tracking plug-in (Fabrice Cordelieres, 2005). The robotic finger was tested with only the FDP tendon pulling and all the other tendons were at rest. The experiment was performed with the variable weights of values from 50 to 300 g with an increasing step of 25 g. Each test was repeated five times.

Fig. 2(e) shows one of the experimental force and velocity results of the robotic finger with a flexible tendon sheath under an external load of 180 g. As can be seen, the fingertip velocity increases at the initial stage and then reaches a quite short plateau, followed by a drop at the end. Using the same approach in the theoretical analysis, the steady-state force and velocity outputs can be obtained (as illustrated in the shadowed block in Fig. 2(e)). The average values of the velocities and forces in this period (0.01 s) were calculated and used as the force–velocity outputs. Assigning the velocity output as the x-value and the force output as the y-value, we obtained one corresponding point in Fig. 2(f). By varying the external loads, a series of (x, y) coordinates can be obtained. And for the robotic finger with flexible tendon sheath, the point cloud of these coordinates is presented in red dots. In addition, a fitted curve of these dots [see the red curve in Fig. 2(f)] is formulated and presented to show the dynamic force–velocity characteristics of the proposed robotic finger. Taking the same procedure, we conducted the tests and collected point cloud data and their rational fitted curves for the robotic fingers with rigid tendon sheaths, as shown in Fig. 2(f), with the yellow, green, and blue curves representing the rigid tendon sheath sizes of 2 mm, 4 mm, and 6 mm, respectively.

As can be seen from both the theoretical [see Fig. 2(d)] and experimental results [see Fig. 2(f)], in terms of the rigid tendon sheaths, the larger the size of the tendon sheath (such as the blue curve representing the tendon sheath of 6 mm), the larger the fingertip output force at low velocity, and the larger the force–velocity workspace. Compared with the fingers with rigid tendon sheaths, under the same condition, the robotic finger with the flexible tendon sheath has a larger fingertip force scale, fingertip velocity scale, and force–velocity workspace, as shown in Fig. 2(d) and (f) with the red curves laying above all the other curves. In the theoretical results shown in Fig. 2(d), the workspace of a robotic finger with the flexible tendon sheath (within the velocity range from 82 to 1600 mm/s) is nearly 41.2% larger than that of a finger with the rigid tendon sheaths on average, with 69.4% larger than the 2 mm size one, 35.5% larger than the 4 mm size one and 18.6% larger than the 6 mm size one. Such a difference is even more significant in the experimental results [see Fig. 2(f)], though the overall fingertip velocity is slightly lower than that of the theoretical results owing to the system friction. In the experimental results, within the velocity range from 80 to 750 mm/s (this range was selected to make sure there were data points on all tendon sheath curves), the workspace of the robotic finger with the flexible tendon sheath is approximately 117.5% larger than that of the fingers with the rigid tendon sheaths on average, specifically 211.1%, 75.6%, and 65.9% larger than the 2 mm, 4 mm, and 6 mm tendon sheaths, respectively. The above results demonstrate a dynamic and consecutive profile to show the force and velocity characteristics that an artificial finger can achieve simultaneously at work. Obviously, the robotic finger with the flexible tendon sheath can work in a larger force–velocity workspace for better interaction with various environments.

Additionally, the quasi-static maximum fingertip force and velocity can be approximately obtained from the dynamic experimental results. For each force–velocity curve in Fig. 2(f), the two ends of the curve give the approximate maximal values of the force and velocity that the finger can generate. To better approach the maximal values without causing too much deviation away from the experiment data, the four fitted force–velocity curves are extended by 5% of the experimental results. The values at the two ends of the extended curves are then selected as the approximate maximum force and velocity, i.e., the quasi-static fingertip force and velocity. Likewise, all the results are normalized with respect to the results of the flexible tendon sheath and are presented as dots of different shapes in Fig. 2(g). As can be seen, in the quasi-static case, the robotic finger with the flexible tendon sheath (the red circle) still shows better force and velocity performance compared with that of the fingers with the rigid tendon sheaths. The experimental results agree well with the theoretical results.

Through the theoretical and experimental studies in this section, it is found that the robotic finger with the flexible tendon sheath provides better quasi-static and dynamic force–velocity characteristics and thus augments the force–velocity workspace

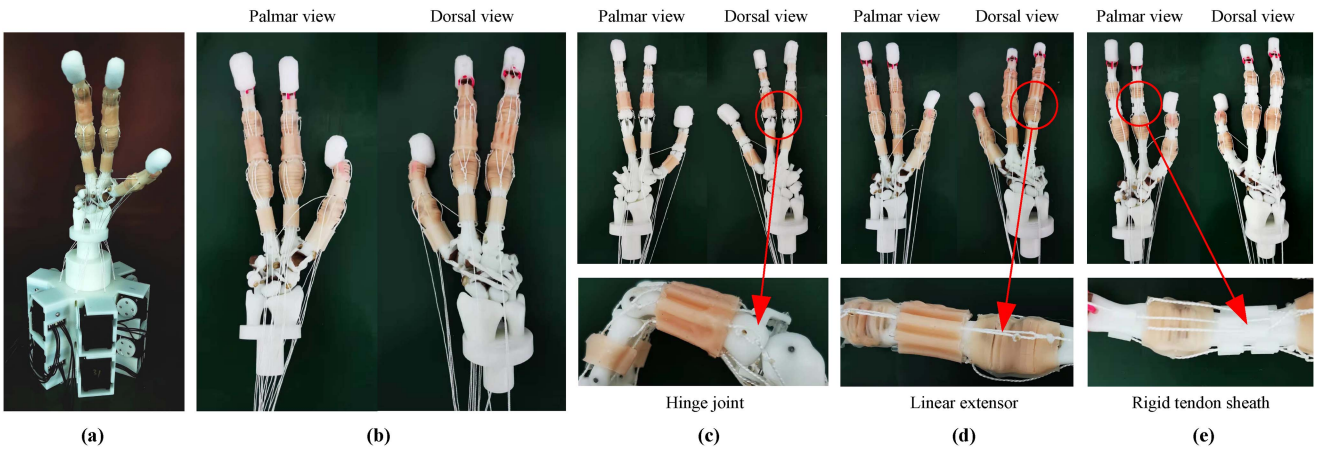

Fig. 3. Physical prototype of a three-fingered robotic hand system and different robotic hand models. (a) Three-fingered robotic hand system; (b) the proposed robotic hand; (c) the robotic hand with hinge joints; (d) the robotic hand with linear extensors; (e) the robotic hand with rigid tendon sheaths.

of the finger. In addition, the results obtained in this study are consistent with the work of O'Brien et al. [5], indicating that the flexible tendon sheaths can serve as a transmission system in a finger to implement the force–velocity self-adaptive morphing that is similar to an elastomeric passive transmission pulley. Hence, the results from this section suggest that the flexible tendon sheath design could be used to replace the complex mechanical transmission system in a robotic finger for the purpose of achieving a large force–velocity workspace.

The above and Part I of this article have studied three biomechanical advantages embedded in human fingers that can be embodied in a robotic finger. To evaluate the overall performance of the proposed robotic finger, a three-fingered robotic hand was developed by using the proposed robotic fingers. And grasping tests on objects of various shapes and materials under the flat, rough, and soft surfaces were conducted in the next section.

IV. Grasping Like Human Fingers

To demonstrate the performance of the robotic finger designed with the aforementioned biomechanical advantages, grasping tests were conducted on a three-fingered robotic hand system shown in Fig. 3(a). The three-fingered robotic hand prototype with the proposed robotic fingers is presented in Fig. 3(b). It contains three of the proposed robotic fingers, one as a thumb, one as an index finger, and one as a middle finger. The whole robotic hand system is actuated by 12 Dynamixel MX-12 W motors. Thereinto, five motors are for the thumb actuation, including one for the abduction, one for the adduction, one for the flexion, and two for the extension. And all the other seven motors are for the index and middle finger actuation, including two for the flexion of the index and middle fingers, two for the extension of the index and middle fingers, one for the abduction of the index finger, one for the abduction of the middle finger, and one for the adduction of the index and middle fingers. Through the power hub and USB2Dynamixel connector, the motors are directly controlled by a PC. The index finger, the middle finger and the thumb were selected to constitute the target testing model because the basic grasping or pick-and-place operation can be normally achieved by these three fingers. It is worth noting that there are no position sensors or tactile sensors on the fingers.

To illustrate the impacts of the ligamentous joint, the reticular extensor and the flexible tendon sheath structures on the robotic hand grasp performance, another three robotic hand prototypes were developed as the comparison group as shown in Fig. 3(c)–(e). Each model in the comparison group has only one kind of structure that is different from the proposed bio-inspired robotic finger design. The hinge joints were employed on the model in Fig. 3(c) to replace the ligamentous joints. The linear extensors were adopted on the model in Fig. 3(d) to compare with the reticular extensors. And the rigid tendon sheaths (2 mm size) were designed on the model in Fig. 3(e) instead of the flexible tendon sheaths. In the experiments, every prototype was mounted on the same actuation platform to complete the grasping tasks.

The grasping tests were conducted on five different objects that were placed on three types of surfaces. The five target objects were selected according to their specific shapes and softness, including a peanut, a pen, a pair of sponge blocks, a piece of tissue, and a playing card. The interaction surfaces were flat, rough, and soft surfaces shown in Fig. 4(a) and (b).

To compare with the human finger grasping performance, six human subjects (male, 25–28 years old) were asked to complete the target grasping tasks with the index finger, the middle finger, and the thumb by using the normal and natural grasping force and posture. Each grasping task was performed ten times, and the corresponding successes and failures were recorded. The human fingers grasp tests are shown in Fig. 4(a), the average success rates of human fingers grasping from six subjects are shown in Fig. 4(c) with the blue line, the orange line, and the grey line representing the results on the flat surface, the rough surface, and the soft surface, respectively.

For the three-fingered robotic hand grasping, a feed-forward control system was constructed through the MATLAB Dynamixel Software Development Kit. And the "teach by showing" programming method was used to operate the hand. The robotic

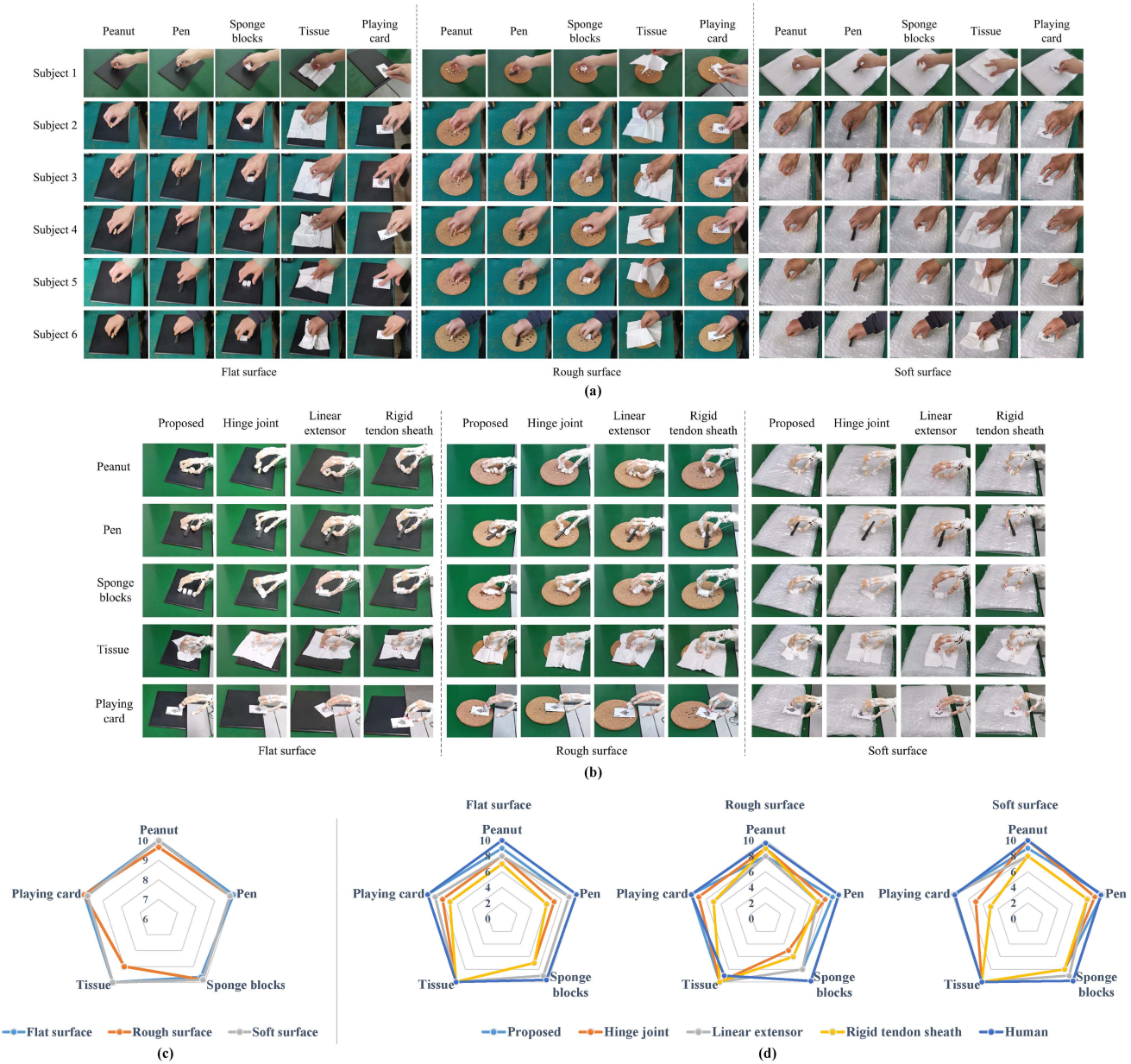

Fig. 4. Grasping test of human and robotic fingers with five target objects on three different surfaces. (a) Grasping tests of human fingers from six subjects; (b) grasping tests of different robotic fingers; (c) the average success rates of human fingers grasping from six subjects; (d) comparison results of the grasping success rates among different robotic fingers and human fingers. Videos of the grasping tests are provided in Appendix A (Extension 1 to 5).

hand was firstly moved to a standard posture by manually rotating the motors to pull the tendons. The motors have embedded position sensors, and all the twelve motors' positions were recorded in a memory that the sequencer would read during playback. It is noted that to avoid the slack phenomenon of the tendon, when all the fingers are in the standard neutral position, there is a pretension force on each tendon, which is generated by manually rotating the motors until all the tendons are straightened. With the same process, the hand was then moved to a desired grasping posture. After that, some minor modifications should be made to generate enough grasping forces by the motors' active actuation. It should be noted that the grasping forces are mainly generated by the FDP tendon contraction of each finger, the other tendons' displacements are only for maintaining the stable grasping motion. With the target object grasped in the robotic hand, the FDP tendon motor was controlled to keep rotating to pull the tendons. Benefitting from the embedded torque sensor in the Dynamixel motor, the torque of the motor can be recorded. It was found that 0.099 N·m motor torque, which could generate 9 N FDP tendon force was enough for all the grasps. Thus, on the basis of the motor's manually rotated position, the FDP tendon motor continued to rotate until the torque reached 0.099 N · m. Then the motors' present positions were recorded, and the present posture of the robotic hand was regarded as the final grasping posture. Here, the sufficient grasping forces could still be considered

TABLE I
AVERAGE GRASPING SUCCESS RATE OF THE HUMAN FINGERS FROM SIX SUBJECTS (OUT OF THE 10-TIME TESTS)

	Flat surface	Rough surface	Soft surface
Peanut	10	9.67	10
Pen	10	9.83	9.83
Sponge blocks	9.67	9.83	9.83
Tissue	10	9	10
Playing card	10	10	9.83

as the results of the motor's position control. Therefore, when the grasping was conducted, the motors could be controlled to move to the recorded positions so as to drive the tendons to make the hand achieve a specific grasping posture with sufficient grasping forces. In this way, all the five objects could be potentially grasped. Each grasping test on all the robotic hands could be deemed to be conducted under the same actuation condition. In addition, the whole robotic hand system was connected with a robotic arm, and the whole grasping process could be demonstrated as four steps. First, the robotic hand was controlled to be opened. Second, the robotic hand was moved downward to approach the target object until it reached the position where the interaction distance was suitable for grasping. Then, the robotic hand was controlled to make the grasp. Finally, the hand was moved up to lift the object. Likewise, each test was repeated 10 times by all these four different robotic hands. The grasping processes are shown in Fig. 4(b), and the corresponding success rates of these tests are shown in Fig. 4(d). In Fig. 4(d), the light blue lines represent the results of the robotic hand with the proposed robotic finger design, the orange lines represent the results of the robotic hand with hinge joints, the grey lines represent the results of the robotic hand with linear extensors, the yellow lines represent the results of the robotic hand with rigid tendon sheaths, and the dark blue lines are the average results of the human fingers which are obtained from Fig. 4(c).

The quality of grasping performance was determined by the collaborative effect of the hand body, the interaction with the target object and the environment, e.g., different surfaces. It can be seen from Fig. 4(c) that the human fingers can achieve quite high grasping success rate in all the grasping tasks, benefitting from their unique structures and intrinsic self-adaptive properties. However, it might be noticed that there are some obvious failures in the tissue and peanut grasping on the rough surface. This could result from the increased friction between the object and the surface and the complex interaction between the fingers and the surface. Moreover, there are some failures during the sponge blocks grasping tests on all the surfaces. The deformable material properties and the uncertain interaction between two sponge blocks could be the reasons. The detailed average grasping success rates of the human fingers are shown in Table I.

For the grasping results of the robotic hands in Fig. 4(d), the overall grasping success rate of the robotic hand with the proposed bio-inspired design is higher than that of the other three robotic hands and quite similar to that of the human fingers. Specifically, on the flat surface, the robotic hand with the proposed design successfully grasped the peanut 9 times, the pen 9 times, the sponge blocks 9 times, the tissue 10 times and the playing card 10 times, respectively, out of the 10-time tests each. Under the same conditions, the robotic hand with hinge joints correspondingly performed 8, 7, 7, 10, and 8 times successful grasps. The robotic hand with linear extensors completed 8, 9, 9, 10, and 9 times successful grasps. And the robotic hand with rigid tendon sheaths shows 7, 6, 7, 10, and 7 times successful grasps. While on the rough and soft surfaces, the average grasping success rate of the three robotic hands in the comparison group dropped more significantly, especially in the sponge blocks and the playing card grasping operations. On the rough surface, the successful grasping cases of the robotic hand with the proposed design appeared 8, 9, 8, 10, and 10 times, respectively, in the peanut, the pen, the sponge blocks, the tissue, and the playing card grasping tests. Correspondingly, the robotic hand with hinge joints had 9, 8, 5, 10, and 9 times successful grasps. The robotic hand with linear extensors had 8, 7, 8, 10, and 7 times successful grasps. And the robotic hand with rigid tendon sheaths had 9, 7, 6, 10, and 7 times successful grasps. On the soft surface, the peanut, the pen, the sponge blocks, the tissue, and the playing card grasping were successfully performed 9, 10, 8, 10, and 10 times by the robotic hand with the proposed design, 10, 9, 8, 10 and 7 times by the robotic hand with hinge joints, 8, 8, 9, 10, and 10 times by the robotic hand with linear extensors, and 8, 8, 8, 10, and 5 times by the robotic hand with rigid tendon sheaths. The detailed grasping success rate results of the robotic hands are shown in Table II.

It can be noticed that all the robotic hands successfully completed the tissue grasping tests by 10 times on all the three surfaces. And the robotic hand with the proposed design completed all the grasp tasks with no less than 8-time success rate out of the 10-time tests. The robotic hand with hinge joints performed worst in the sponge blocks grasping tests on the rough surface, with only five times successful grasps. It may be due to the fact that the sponge blocks will be compressed and deformed when they are grasped. The complex interaction forces between the two sponge blocks will make them quite easily bound out if there are no stable enough external forces to maintain their status. Compared with the ligamentous joint, the hinge joint cannot provide high joint stiffness to make the grasping stable. The fingers' posture can be easily changed by the counterforce during grasping, resulting in the bounding out behavior of the sponge blocks. Besides, the rough surface is more likely to influence the grasping posture of the robotic hand with hinge joints, leading to a case of failure. As to the robotic hand with linear extensors, it performed well on both flat and soft surfaces. However, on the rough surface, the overall success rates are a little bit lower. The reason could possibly be that the rough surface more easily causes the interference during the grasping interaction due to the reduced fingertip force resulting from the linear extensor. For example, during the pen grasping, the interference from the rough surface causes the improper finger grasping positions on the pen body. This will introduce the additional gravity torque, which the fingers with linear extensors cannot generate sufficient grasping forces and torques to resist.

TABLE II
GRASPING SUCCESS RATE OF THE ROBOTIC HANDS (OUT OF THE 10-TIME TESTS)

(a) Flat surface

	Proposed	Hinge joint	Linear extensor	Rigid tendon sheath
Peanut	9	8	8	7
Pen	9	7	9	6
Sponge blocks	9	7	9	7
Tissue	10	10	10	10
Playing card	10	8	9	7

(b) Rough surface

	Proposed	Hinge joint	Linear extensor	Rigid tendon sheath
Peanut	8	9	8	9
Pen	9	8	7	7
Sponge blocks	8	5	8	6
Tissue	10	10	10	10
Playing card	10	9	7	7

(c) Soft surface

	Proposed	Hinge joint	Linear extensor	Rigid tendon sheath
Peanut	9	10	8	8
Pen	10	9	8	8
Sponge blocks	8	8	9	8
Tissue	10	10	10	10
Playing card	10	7	10	5

TABLE III
GRASPING SUCCESS RATES OF THE ROBOTIC HANDS NORMALIZED WITH RESPECT TO THOSE OF THE PROPOSED MODEL

(a) Flat surface (out of the total 50-time tests)

	Proposed	Hinge joint	Linear extensor	Rigid tendon sheath
Success rates	47	40	45	37
Normalized percentage	1	85%	96%	79%

(b) Rough surface (out of the total 50-time tests)

	Proposed	Hinge joint	Linear extensor	Rigid tendon sheath
Success rates	45	41	40	39
Normalized percentage	1	91%	89%	87%

(c) Soft surface (out of the total 50-time tests)

	Proposed	Hinge joint	Linear extensor	Rigid tendon sheath
Success rates	47	44	45	39
Normalized percentage	1	94%	96%	83%

(d) All the surfaces (out of the total 150-time tests)

	Proposed	Hinge joint	Linear extensor	Rigid tendon sheath
Success rates	139	125	130	115
Normalized percentage	1	90%	94%	83%

Among all the robotic hands, the robotic hand with rigid tendon sheaths showed the worst grasping performance. The reduced fingertip forces and the weakened passive behaviour could be the most likely reasons. For instance, the pen grasping necessitates high demands on fingertip forces, where the failures are more common. With the rigid tendon sheaths, the fingers cannot easily achieve a proper grasping posture due to the poor interaction capability with the external environment. This behavior could be clearly observed during the playing card grasping tests. To successfully grasp the card, the fingers should touch the card and move it backward to the palm along the surface, forming a proper grasping posture. This motion cannot be well performed only by the fingers' active actuation. The fingers should be able to passively deform during the interaction with the card and the surface. Otherwise, the conflict between the fingers' active motion and the surface will lead to grasping failures. The flexible tendon sheaths could offset the passive deformation of the finger, but the rigid tendon sheaths could not.

To better show the enhanced grasping performance of the hand with the proposed robotic finger, the grasping success rates on each interaction surface of the robotic hands in the comparison group were normalized with respect to those of the proposed model. For each surface, the successful grasping cases of all the five objects performed by a certain robotic hand were summed up as the evaluation of its grasping performance on this surface. The results are shown in Table III(a)–(c). Specifically, on the flat surface, the robotic hand with hinge joints, linear extensors, and rigid tendon sheaths can achieve 85%, 96%, and 79% of the grasping success rates of the proposed model, respectively. In this case, the rigid tendon sheaths and the hinge joints structures had more adverse impacts on the grasping performance. On the rough surface, the robotic hands in the comparison group can respectively achieve 91%, 89%, and 87% of the grasping success rates of the proposed hand. In such a condition, the structures of hinge joints, linear extensors and rigid tendon sheaths produced negative impacts on grasping to a similar degree. The corresponding normalized percentage goes to 94%, 96%, and 83% on the soft surface, where the robotic hand with rigid tendon sheaths had the worst performance. From the view of the whole grasping tests on the robotic hands [see Table III(d)], obviously, the robotic hand with the proposed design still performed better than the other robotic hands in the comparison group. Compared with the proposed model, the overall grasping performance of

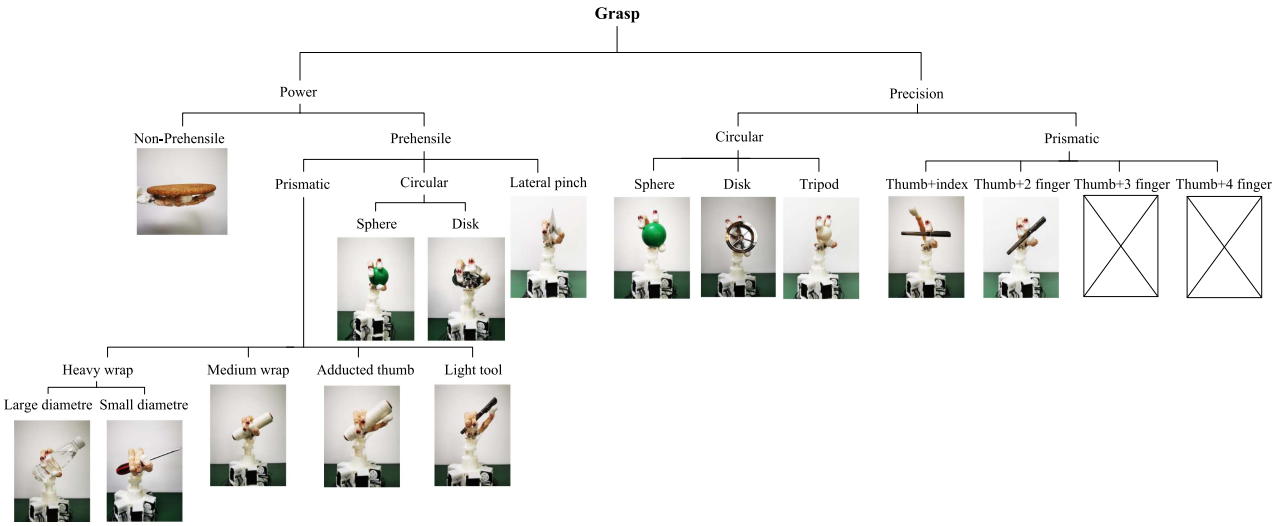

Fig. 5. Cutkoskey grasp taxonomy of the proposed robotic hand.

TABLE IV
GRASPING SUCCESS RATES OF THE HAND WITH PROPOSED ROBOTIC FINGERS NORMALIZED WITH RESPECT TO THOSE OF THE HUMAN FINGERS

		Proposed fingers	Human fingers
Flat surface	Success rates	47	49.67
	Normalized percentage	95%	1
Rough surface	Success rates	45	48.33
	Normalized percentage	93%	1
Soft surface	Success rates	47	49.5
	Normalized percentage	95%	1
All the surfaces	Success rates	139	147.50
	Normalized percentage	94%	1

TABLE V
MULTIMEDIA EXTENSIONS (INCLUDING TESTS ON HUMAN FINGERS AND FOUR THREE-FINGERED ROBOTIC HANDS WITH DIFFERENT STRUCTURES)

Extension	Media type	Description
1	Video	Nipping a peanut
2	Video	Picking up a pen
3	Video	Pinching two sponge blocks
4	Video	Snatching up a piece of tissue
5	Video	Drawing a playing card
6	Video	Overview of the three-fingered robotic hand

the robotic hand with hinge joints, linear extensors, and rigid tendon sheaths decreases by 10%, 6%, and 17%, respectively. The results evidence that the proposed bio-inspired design could enhance the robotic hand's grasping capabilities, especially the flexible tendon sheath and the ligamentous joint design.

Besides, to further show the human-finger-like grasping performance of the proposed model, the success rates of the proposed robotic hand are normalized with respect to those of the human fingers, shown in Table IV. The list of videos for grasping performance with robotic hands with different structures are listed in Table V, with the associated videos supplied in the supplemental materials. It can be seen that the robotic hand with the proposed bio-inspired robotic fingers can achieve over 90% grasping performance of the human fingers on all the three surfaces, with the average performance showing 94%. Overall, despite the grasping difficulties introduced by the target objects and the environments, our robotic fingers and human fingers could both cope with them very well. However, the human hand can complete many other grasps. The Feix and Cutkoskey grasp taxonomies have been widely used to demonstrate the grasping capabilities of the human and the robotic hand. Given that the hand model only has three fingers, the Cutkoskey taxonomy was adopted to validate its human-finger-like grasping performance. The results are shown in Fig. 5. In the total of 16 types of grasps, the three-fingered robotic hand completed nearly all the types (the two missing ones could have been accomplished with two additional fingers). These tests have successfully demonstrated that the adopted structural design and materials of our robotic finger could generate the human-finger-like grasping capability. In the experiments, there are no tactile sensors used, and there is no complex control system or planning algorithm involved, however, the proposed three-fingered robotic hand can still show excellent grasping performance similar to human fingers. Hence, it indicates that by considering the biomechanical advantages in the robotic hand design, it can not only improve the overall grasping performance, but also reduce complexity in the control system and simplify the planning and computation load.

V. Discussions

Building a robotic hand with the fantastic functionality to grasp and manipulate objects like a human hand has always been a dream for robotics research. By carefully studying the musculoskeletal system of the human finger, this article developed a multilayer anthropomorphic robotic finger, which aims to embody human-finger-like biomechanical advantages and grasping performance, shedding light on the better design of robotic fingers and hands. Through the theoretical modelling and experimental study in Part I and Part II of this article, we have demonstrated that the human-finger-like biomechanical advantages and grasping capabilities can be achieved in a robotic finger through sophisticated bio-inspired design based on the understanding of biomechanics of the human finger.

A. Biomechanical Advantages

Referring to the previous study, the biomechanical advantages of human hands are mainly associated with the biological joints [18], [19], the extensor mechanisms [20], [21] and the pulley-like tendon sheaths [10], [12]. Notwithstanding the great progress already made, some specific biomechanical advantages have not been clearly clarified or interpreted. Especially, when we talk about the biomimetic robotic hand design, it mostly relates to mimic the biological structures, hardly touching the biomechanical advantages. The biomechanical advantages embedded in the ligamentous joint and the extensor mechanism have been comprehensively illustrated in Part I of this article.

With the corresponding bio-inspired design, the robotic finger can achieve anisotropic variable joint stiffness and enlarged fingertip feasible force space. This part reveals that the augmented force–velocity workspace can be realized in the proposed robotic finger due to the implementation of the flexible tendon sheaths. The larger force–velocity workspace means a larger range of force and velocity can be provided automatically and continuously according to various demands and situations owing to the self-morphing of the flexible tendon sheaths, and hence the finger has better manipulability and dexterity. Taking the baseball catch as an example, our hand needs to close rapidly to catch the ball at the moment the ball touches the hand. Sufficient grasping forces are then needed to hold the ball so that it won't fall off from the hand. The whole process happens in a very short time, and our hand needs to quickly adjust from the high-velocity mode to the high-torque mode according to the external load. Such a process can put a heavy burden on the control system of the conventional robotic hands, in which both fingertip force and velocity need to be controlled to make instantaneous changes. However, the flexible tendon sheaths could simplify the complex control problem by self-adaptive morphing so as to autonomously adjust the moment arm of the joint without reliance on any control or sensing system. This is a typical instance showing the mechanical intelligence of the biological body. The mathematical model established in this article is the very first attempt to theoretically investigate the behavior of the flexible tendon sheath, providing a theoretical method for analysing this kind of mechanism. From this article, it can be found that by approximately replicating the pulley-like flexible tendon sheaths in the robotic finger, better quasi-static and dynamic force–velocity characteristics were obtained. These results supplement the findings on the functions of the tendon sheath structures in human fingers, revealing another significant function apart from constraining the tendons [10], [11]. Moreover, different from the elastomeric passive transmission systems design in the research of O'Brien et al. [5], the force–velocity self-adjustment of the robotic finger in this article was realized by the smart flexible tendon-sheath structure design on the finger body rather than adding any other components in the mechanical transmission system, which greatly simplifies the design of the whole robotic system.

In addition, with the proposed biomimetic design, more characteristics of the human finger can be exploited in the robotic finger. Taking the biological joint as an example, together with the articular bones, the capsuloligamentous structure forms a tension-compression body, such that compression pressures will only be exerted onto the bones, and tensions will only be loaded on the joint ligaments and capsules. The unique joint structure allows not only the flexion-extension and the abduction-adduction motions, but also the supination-pronation motion [18]. This improved dexterity leads to better interaction between fingers and objects. Further, to prevent irreparable damage from unexpected external impacts, the joints can be dislocated out of their normal position and be easily repaired through joint reduction [22]. As to the flexible tendon sheaths, they can also enhance the passive behaviors of the fingers. For instance, passive deformation of the tendons and muscles is demanded when the posture of a finger tends to be changed by an external disturbance. Such deformation can be partially compensated through the tendon sheath's adjustment to the joint moment arm, leading to a simplified control for the tendon–muscle system. This behaviour could be observed in the grasping tests.

The bio-inspired robotic finger designed in this article provides new insights into biomechanical advantages that other robotic fingers/hands have rarely demonstrated. In terms of the joint stiffness property, the conventional robotic hands with hinge joints could hardly possess variable joint stiffness [23], [24], including the metamorphic robotic hand with increased degrees of freedom [25], [26], [27], [28]. The recent robotic hands with elastic joints often used rubber-like materials or springs, which traded away high joint stiffness for enhancing hand dexterity [29], [30]. The variable joint stiffness could have been potentially well achieved and demonstrated in the biomimetic ligamentous joint design in several anthropomorphic robotic hands [12], [13], [15], [19], but no sufficient study or evidence has been presented. As for the function of the extensor mechanism, a few novel biomimetic robotic hands tended to adopt the extensor mechanism structure [12], [14], [21], [31]. However, limited investigation has been carried out to study the mechanical outputs, especially the feasible force space of robotic fingers, that can be benefited from such a structure. Likewise, a number of tendon-driven robotic hands adopted the design of tendon sheaths or pulleys, but most of these robotic hands made this structure rigid only for guiding the tendon routes [13], [14], [23], [24], [32], [33]. Some bio-inspired robotic hands used flexible tendon sheaths so as to highly mimic the

human hand structure [12], [15]. These flexible tendon sheaths did help improve the performance of robotic hands, but no detailed analysis, investigation or verification were addressed. In this paper, these biomechanical advantages were systematically investigated, simulated, verified, and eventually demonstrated based on the proposed robotic finger, theoretically and experimentally. The results have indicated that, by considering the biomechanical properties in the robotic finger design, the desired human-finger-like advantages such as anisotropic variable joint stiffness, enlarged feasible force space, and augmented force-velocity workspace can be achieved. Through the grasping tests at the end of the research, the biomechanical advantages embedded in the design of the proposed robotic finger are proved to help enhance the grasping capability, especially the self-adaptive morphing property of the flexible tendon sheath.

A human only has two hands to cope with the immense amount of daily activities. Except for the sophisticated neural control and sensing systems, the mechanical properties of the physical body also play significant roles. As having been pointed out by Pfeifer et al. [34], [35], physical constraints form the dynamics of the interaction of the embodied systems with their environments, and the better design of the mechanical system can reduce the control complexity and relieve the computing burden [36] in the robotic systems. With the biomechanical advantages embedded in the biomimetic structures, even without the complex control or sensing system, the robotic fingers can generate comparable grasping performance to human fingers, indicating the properties of the proposed robotic finger as adaptivity, versatility, and dexterity.

B. Limitation and Future Work

The mathematical model of the flexible tendon sheaths system was simplified and more sophisticated models need to be further developed, and more accurate results could be obtained through computational modelling. Furthermore, except for the grasping capability, the manipulation capability could be explored and demonstrated to better illustrate the advantages of the proposed robotic finger design. Based on the robotic finger in this research, the whole robotic hand model with five fingers and skin will be developed in the future.

VI. Conclusion

This article for the first time systematically investigated and demonstrated that three intrinsic human-finger-like biomechanical advantages can be achieved in a bio-inspired robotic finger. The mathematical modeling and experimental verification approaches were both employed. Particularly in this part, the method of solving differential equations was implemented to present the self-adaptive morphing behaviors of the flexible tendon sheaths that could regulate and augment the force–velocity workspace of the finger automatically. All the theoretical results were then verified by the experimental results based on the tests that were carried out on the proposed robotic finger. The results have shown that variable anisotropic finger joint stiffness (see Part I), enlarged fingertip feasible force space (see Part I), and augmented fingertip force–velocity workspace could be achieved by integrating the biomechanical advantages in the robotic finger through biomimetic design. To further prove that our highly biomimetic design could benefit the grasping performance, four three-fingered robotic hands (one with the proposed design, one with hinge joints, one with linear extensors, and one with rigid tendon sheaths) were then developed and tested. All the robotic hands have no complex control and sensing systems. Grasping tests on objects of various shapes and materials on flat, rough, and soft surfaces were conducted. The results have shown that the robotic hand developed based on the proposed robotic finger could achieve higher grasping success rates compared with the robotic hands with hinge joints, linear extensors, and rigid tendon sheaths. And it could achieve comparable grasping performance to human fingers. It is evident that by properly integrating the biomechanical advantages of biological organisms in the robotic system design, even without adopting a complicated control system or learning approach, the robotic system could still achieve excellent performance that could normally be witnessed from human operations, with the desirable properties like adaptivity, versatility, robustness, and dexterity. From the view of biomechanics, this article provided a theoretical and experimental background for the development of a new generation of robotic finger/hand that may be able to achieve the fantastic functions of human hands.

The work presented in this article can provide some insights into the robotic finger/hand design. To obtain human-finger-like biomechanical advantages and enhanced grasping capabilities, the ligamentous joints, the reticular extensor mechanism structures and the flexible tendon sheaths are strongly recommended to be adopted in the robotic finger/hand design. For the ligamentous joints, PET braided ribbons were selected as the artificial ligaments of the proposed design since their fiber materials and micro-structures enabled them to possess similar load-deformation properties to human finger ligaments. The origins and insertions of the ligaments can be found by referring to their corresponding locations in human finger joints, and using the mathematical model in this paper to accordingly adjust and optimize a specific design. Besides, to improve the stability of the joints without bringing too much tension resistance, we adopted silicone–rubber-made capsules with wrinkle structures to cover outside the joint ligaments. As to the reticular extensor mechanism structures, we used the fishing-line tendons to fabricate the extensor network owing to their high strength and low friction resistance. The whole extensor mechanism structure was weaved according to the simplified morphology abstracted from Winslow's tendinous rhombus model. Further, flexible tendon sheaths are highly recommended in robotic finger/hand design. Silicone rubber and the moulding process were used in the fabrication of this proposed robotic finger, due to the moderate tensile strength, elasticity, and elongation properties of the silicone rubber. Inside the silicone rubber tendon sheath tunnels, there were flexible PTFE tubes providing smooth contacts for the tendon motion, which are indispensable for the whole flexible tendon sheath structures.

Appendix
Index to Multimedia Extensions

The videos are in the Supplementary Materials.

ACKNOWLEDGMENT

The authors would like to thank D. P. Connor, A. R. J. Dunbar, H. Yang and L. Yan for assisting 3D printing the parts, and Y. Wei and B. Zhou for their insight and discussion throughout this work.

REFERENCES

[1] C. Piazza, G. Grioli, M. G. Catalano, and A. Bicchi, "A century of robotic hands," *Annu. Rev. Control*, Robot., Auton. Syst., vol. 2, pp. 1–32, 2019.
[2] E. Azizi, E. L. Brainerd, and T. J. Roberts, "Variable gearing in pennate muscles," in *Proc. Nat. Acad. Sci.*, 2008, pp. 1745–1750.
[3] J. Alcazar, R. Csapo, I. Ara, and L. M. Alegre, "On the shape of the force-velocity relationship in skeletal muscles: The linear, the hyperbolic, and the double-hyperbolic," *Front. Physiol.*, vol. 10, 2019, Art. no. 769.
[4] H. Asada and I. H. Ro, "A linkage design for direct-drive robot arms," *J. Mechanisms, Transmissions, Automat. Des.*, vol. 107, no. 4, pp. 536–540, 1985.
[5] K. W. O'Brien et al., "Elastomeric passive transmission for autonomous force-velocity adaptation applied to 3D-printed prosthetics," *Sci. Robot.*, vol. 3, no. 23, 2018, Art. no. eaau5543.
[6] A. V. Hill, "The heat of shortening and the dynamic constants of muscle," in *Proc. Roy. Soc. London. Ser. B-Biol. Sci.*, 1938, pp. 136–195.
[7] B. C. Abbott and D. R. Wilkie, "The relation between velocity of shortening and the tension-length curve of skeletal muscle," *J. Physiol.*, vol. 120, no. 1–2, pp. 214–223, 1953.
[8] D. F. B. Haeufle, M. Günther, R. Blickhan, and S. Schmitt, "Proof of concept of an artificial muscle: Theoretical model, numerical model, and hardware experiment," in *Proc. IEEE Int. Conf. Rehabil. Robot.*, 2011, pp. 1–6.
[9] S. Schmitt, D. F. B. Haeufle, R. Blickhan, and M. Günther, "Nature as an engineer: One simple concept of a bio-inspired functional artificial muscle," *Bioinspiration Biomimetics*, vol. 7, no. 3, 2012, Art. no. 0 36022.
[10] A. A. Amis and M. M. Jones, "The interior of the flexor tendon sheath of the finger. the functional significance of its structure," *J. Bone Joint Surg. Brit. Volume*, vol. 70, no. 4, pp. 583–587, 1988.
[11] G.-T. Lin, W. P. Cooney, P. C. Amadio, and K.-N. An, "Mechanical properties of human pulleys," *J. Hand Surg.*, vol. 15, no. 4, pp. 429–434, 1990.
[12] Z. Xu and E. Todorov, "Design of a highly biomimetic anthropomorphic robotic hand towards artificial limb regeneration," in *Proc. IEEE Int. Conf. Robot. Automat.*, 2016, pp. 3485–3492.
[13] M. Chepisheva, U. Culha, and F. Iida, "A biologically inspired soft robotic hand using chopsticks for grasping tasks," in *Proc. Int. Conf. Simul. Adaptive Behav.*, 2016, pp. 195–206.
[14] A. A. M. Faudzi, J. Ooga, T. Goto, M. Takeichi, and K. Suzumori, "Index finger of a human-like robotic hand using thin soft muscles," *IEEE Robot. Automat. Lett.*, vol. 3, no. 1, pp. 92–99, Jan. 2017.
[15] M. Tebyani et al., "3D printing an assembled biomimetic robotic finger," in *Proc. 17th Int. Conf. Ubiquitous Robots*, 2020, pp. 526–532.
[16] A. J. Van Soest and M. F. Bobbert, "The contribution of muscle properties in the control of explosive movements," *Biol. Cybern.*, vol. 69, no. 3, pp. 195–204, 1993.
[17] D. F. B. Haeufle, S. Grimmer, and A. Seyfarth, "The role of intrinsic muscle properties for stable hopping– stability is achieved by the force–velocity relation," *Bioinspiration Biomimetics*, vol. 5, no. 1, 2010, Art. no. 0 16004.
[18] E. Y. Chao, *Biomechanics of the Hand: A Basic Research Study*. Singapore: World Scientific, 1989.
[19] J. Hughes, P. Maiolino, and F. Iida, "An anthropomorphic soft skeleton hand exploiting conditional models for piano playing," *Sci. Robot.*, vol. 3, no. 25, 2018, Art. no. eaau3098.
[20] F. J. Valero-Cuevas, F. E. Zajac, and C. G. Burgar, "Large index-fingertip forces are produced by subject-independent patterns of muscle excitation," *J. Biomech.*, vol. 31, no. 8, pp. 693–703, 1998.
[21] D. D. Wilkinson, M. V. Weghe, and Y. Matsuoka, "An extensor mechanism for an anatomical robotic hand," in *Proc. IEEE Int. Conf. Robot. Automat.*, 2003, pp. 238–243.
[22] Y.-S. Seo et al., "Human-mimetic soft robot joint for shock absorption through joint dislocation," *Bioinspiration Biomimetics*, vol. 15, no. 1, 2019, Art. no. 0 16001.
[23] S. C. Jacobsen, J. E. Wood, D. F. Knutti, and K. B. Biggers, "The utah/mit dextrous hand: Work in progress," *Int. J. Robot. Res.*, vol. 3, no. 4, pp. 21–50, 1984.
[24] "Shadow dexterous hand technical specification," Feb. 2019, Accessed Jun. 5, 2021. [Online]. Available: https://www.shadowrobot.com/dexterous-hand-series/
[25] J. S. Dai and D. Wang, "Geometric analysis and synthesis of the metamorphic robotic hand," *J. Mech. Des.*, vol. 129, no. 11, pp. 1191–1197, 2007.
[26] J. S. Dai, D. Wang, and L. Cui, "Orientation and workspace analysis of the multifingered metamorphic hand–metahand," *IEEE Trans. Robot.*, vol. 25, no. 4, pp. 942–947, Aug. 2009.
[27] G. Wei, J. S. Dai, S. Wang, and H. Luo, "Kinematic analysis and prototype of a metamorphic anthropomorphic hand with a reconfigurable palm," *Int. J. Humanoid Robot.*, vol. 8, no. 3, pp. 459–479, 2011.
[28] E. Emmanouil, G. Wei, and J. S. Dai, "Spherical trigonometry constrained kinematics for a dexterous robotic hand with an articulated palm," *Robotica*, vol. 34, no. 12, pp. 2788–2805, 2017.
[29] R. Deimel and O. Brock, "A novel type of compliant and underactuated robotic hand for dexterous grasping," *Int. J. Robot. Res.*, vol. 35, no. 1–3, pp. 161–185, 2016.
[30] G. P. Kontoudis, M. V. Liarokapis, A. G. Zisimatos, C. I. Mavrogiannis, and K. J. Kyriakopoulos, "Open-source, anthropomorphic, underactuated robot hands with a selectively lockable differential mechanism: Towards affordable prostheses," in *Proc. IEEE/RSJ Int. Conf. Intell. robots Syst.*, 2015, pp. 5857–5862.
[31] A. D. Deshpande, R. Balasubramanian, J. Ko, and Y. Matsuoka, "Acquiring variable moment arms for index finger using a robotic testbed," *IEEE Trans. Biomed. Eng.*, vol. 57, no. 8, pp. 2034–2044, Aug. 2010.
[32] A. D. Deshpande et al., "Mechanisms of the anatomically correct testbed hand," *IEEE/ASME Trans. Mechatronics*, vol. 18, no. 1, pp. 238–250, Feb. 2011.
[33] F. Lotti, P. Tiezzi, G. Vassura, L. Biagiotti, G. Palli, and C. Melchiorri, "Development of UB hand 3: Early results," in *Proc. IEEE Int. Conf. Robot. Automat.*, 2005, pp. 4488–4493.
[34] R. Pfeifer, M. Lungarella, and F. Iida, "Self-organization, embodiment, and biologically inspired robotics," *Science*, vol. 318, no. 5853, pp. 1088–1093, 2007.
[35] R. Pfeifer, F. Iida, and M. Lungarella, "Cognition from the bottom up: On biological inspiration, body morphology, and soft materials," *Trends Cogn. Sci.*, vol. 18, no. 8, pp. 404–413, 2014.
[36] A. Billard and D. Kragic, "Trends and challenges in robot manipulation," *Science*, vol. 364, no. 6446, 2019, Art. no. eaat8414.

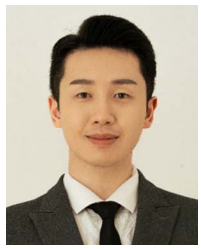

Yiming Zhu received the Ph.D. degree in mechanical engineering from the University of Manchester, Manchester, U.K., in 2021.

He is currently a Lecturer of intelligence mechanics with the College of Intelligence Science and Technology, National University of Defense Technology, China. His research interests include biorobotics and biomechanics, particularly the biomimetic robotic hand development.

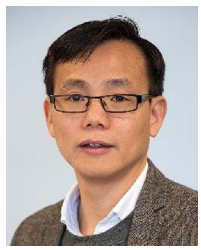

Guowu Wei (Member, IEEE) received the Ph.D. degree in robotics from King's College London, London, U.K., in 2012.

He is a Lecturer of robotics and mechanical engineering with the School of Science, Engineering and Environment, University of Salford, Salford, U.K. He has more than 120 peer-reviewed publications. His research was funded by EPSRC, EU-FP7, ICUK, NSFC, and Royal Academy of Engineering. His research interests include robotics, mechatronics, and manipulation and grasping, reconfigurable mechanisms and robotics, and biorobotics.

Dr. Wei serves as the Associate Editor for *Robotica, and Journal of Mechanical Engineering Science, Topic Editor for Mechanical Science*, Academic Editor for *Applied Bionics and Biomechanics*, and Associate Editor for IEEE/RSJ International Conference on Intelligent Robots and Systems (IROS) and IEEE International Conference on Robotics and Automation (ICRA). He is currently the Deputy Chair of IFToMM MO U.K.

Lei Ren (Member, IEEE) received the Ph.D. degree in biomechanical engineering from the University of Salford, Manchester, U.K., in 2005.

He is is the leader of Biomechanics Specialism at Department of Mechanical, Aerospace and Civil Engineering, University of Manchester, and is also with the Key Laboratory of Bionic Engineering, Ministry of Education, Jilin University. He researches in the field of biorobotics and biomechanics, including humanoid locomotion, hand grasping and manipulation, bioinspired limb prosthetics etc. He has been the PI and Co-I of over 30 research projects funded by EPSRC, BBSRC, NSFC, MoST etc. He has over 280 peer-reviewed publications, and has been awarded over 120 patents. His research works have been reported by Nature, Science News, Wired, Telegraph, Science Daily and BBC etc.

Prof. Ren is the Deputy General Secretary of the International Society of Bionic Engineering (ISBE), sits in the Council of Chairs, Biomedical Engineering Society (BMES). He also serves as the associate editor-in-chief of *Journal of Bionic Engineering*, the associate editors of *Frontiers in Bioengineering and Biotechnology*, and the editorial members of *Frontiers of Mechanical Engineering, Journal of Healthcare Engineering, Chinese Journal of Mechanical Engineering* etc.

Zirong Luo received the Ph.D. degree in mechanical engineering from National University of Defense Technology (NUDT), Changsha, China, in 2010.

He is currently a Professor of mechanical engineering with the College of Intelligence Science and Technology, NUDT. He has authored or coauthored more than 80 peer-reviewed publications, and has been awarded more than 50 related patents. His current research interests include unmanned system, mobile robots, wave energy, bio-inspired robots and micro robots.

Jianzhong Shang received the Ph.D. degree in mechanical engineering from Huazhong University of Science and Technology, Wuhan, China, in 2006.

He is currently the Professor and Doctoral Supervisor with the College of Intelligence Science and Technology, National University of Defense Technology, China. His research interests include mechanical engineering, including robotics, biomechanics, digital design and manufacturing, and has more than 100 peer-reviewed publications.

Prof. Shang has been awarded the Second Prize of National Science and Technology Progress.